JOURNAL OF COMPUTATIONAL PHYSICS **124,** 71–84 (1996)
ARTICLE NO. 0045

A Second-Order Accurate Implicit Scheme for Strongly Coupled Fluid Equations Applied to Fluid Electron Turbulence in a Magnetised Plasma

BRUCE D. SCOTT

Max Planck Institut für Plasmaphysik, EURATOM Association, D-85748 Garching, Germany

Received March 6, 1995

A computational method for treating fluid-type turbulence with strongly coupled equations is outlined and tested. Applied to drift wave turbulence in a magnetised plasma, it is generalisable to other systems. Coupling operators are treated with the second-order accurate scheme DIRK2, in which only values at the current time step are needed to advance the system. Turbulent advection, small-scale dissipation, and weak forcing terms are split apart and treated independently, so that the overall scheme is still first order. Nevertheless, the part that is not second order is that which needs to be resolved in any case. Strict convergence and error testing shows the new scheme to outperform the implicit one previously used with drift wave turbulence by a significant margin.

I. INTRODUCTION

In many computational fluid systems, the practitioner faces the problem of dissipative coupling between two or more of the dependent variables and the coupling operator is rapidly varying with position. When the coupling is weak the variables evolve independently, and when it is strong a subset of the variables evolves independently with the others following equilibrium relations. One example is a reacting flow in which some of the reaction rates are arbitrarily fast in some regions of the computational domain but are slow enough that they must be followed in others. In the physical system described below the problem is exacerbated by the fact that one of the dependent variables appears under the time derivative with the Laplacian operator. The generic form of the system is

$$\frac{\partial}{\partial t}\nabla^2\phi - \alpha_{11}\phi + \alpha_{12}n + \alpha_{13}T = S_1, \tag{1}$$

$$\frac{\partial n}{\partial t} - \alpha_{21}\phi + \alpha_{22}n + \alpha_{23}T = S_2, \tag{2}$$

$$\frac{\partial T}{\partial t} - \alpha_{31}\phi + \alpha_{32}n + \alpha_{33}T = S_3, \tag{3}$$

where ϕ, n, and T are the dependent variables, the α's are coupling operators which are in general variable, the S's are arbitrary forcing terms, and the system is defined on a two-dimensional Cartesian grid, (x, y). It is not always true that both dimensions involved in ∇^2 can be Fourier transformed away; indeed, in the case described below only the y-direction is transformed, and the α's are specified functions of x and the Fourier mode index for the y-coordinate. The matrix of the α's is not, in general, definite and may be singular.

The difficulty in this system is apparent when these α's are rapidly varying, since the Laplacian operator in Eq. (1) couples the regions in x which are characterised by weak and strong coupling. It is important not to let this variability of the α's affect the x-dependence of ϕ, n, and T in a spurious way. An implicit time-stepping algorithm for this system was previously developed in the case of two dependent variables, ϕ and n [1]. The algorithm was only first-order accurate, and the time step was limited accordingly. In this paper the second-order accurate stepping algorithm known as DIRK2 [2] is applied to the system for four equations, and it is indeed found to be second-order accurate with no spurious transport in the x-direction; i.e., its performance is not damaged by the presence of the Laplacian operator. The physical milieu which makes this an important problem to solve in the present case is the phenomenon of anomalous transport in fusion plasmas, which may find an eventual explanation in terms of the turbulent dynamics of the electron fluid in a magnetised plasma, in general.

In the last decade or so there has been much experimental activity directed towards understanding the details of the turbulent fluctuations in density ($\tilde{n}$), temperature ($\tilde{T}$), and electrostatic potential ($\tilde{\phi}$), which are ubiquitous in tokamak plasma discharges [3]. Direct *in situ* measurements with Langmuir probes in the relatively cool edge regions ($T \lesssim 50$ eV) have shown that the turbulence is at a level consistent with the proposition that it is responsible for the anomalous transport of particles and energy oc-

0021-9991/96 $18.00

curring in those regions. Since anomalous transport (transport rates several orders of magnitude larger than they would be if caused by interparticle collisions) is also ubiquitous in laboratory fusion experiments, in all regions, understanding its mechanism is generally recognised as one of the central problems outstanding in the magnetic fusion effort. Among the important results so far obtained from the experiments are: (a) Dynamics at ''drift scales'': both spatial and temporal scales are commensurate with electron drift-wave dynamics. That is, particle flows occur according to the E $\times$ B velocity, $\mathbf{v}_E = (c/B^2)\ \mathbf{E} \times \mathbf{B}$, and the electron thermal energy is responsible for the turbulence. (b) Strong departures from adiabatic behaviour in the electrons, where ''adiabatic'' connotes strict adherence to a Boltzmann distribution. For small fluctuations it would mean $\tilde{n}/n \to e\tilde{\phi}/T$ and $\tilde{T} \to 0$. What is observed is that all three fluctuations are of the same magnitude (with $\tilde{T}/T$ somewhat smaller) and have large phase shifts relative to one another. (c) Spectral energy transfer dynamics proceeding in both directions with roughly equal importance: smaller to larger scales and vice versa [4]. This is in marked contrast to the usual situation in experiments with neutral fluids and implies that more than one type of nonlinearity is concurrently important. (d) Indications of a transport mechanism which is both nondiffusive and nonlocal. Here, ''nondiffusive'' implies that transport does not have the simple scaling with gradients that collisional transport does, and with more than one gradient present a quantity can be transported in the direction of its gradient [5]. ''Nonlocal'' implies that the level and character of the turbulence at a given radial position depends on conditions within a range of that position quite a bit larger than the characteristic scale of the turbulence, and a change in regime at one position can cause the turbulence level to drop everywhere within such a large range [6].

Obviously, there is more to the physics of this state of affairs than is intuitive, and it has become imperative to simulate the dynamics of a system of equations describing the electrons as completely as possible [7]. The principle difficulty in doing this is the speed of the electron dynamics parallel to the magnetic field. In the fluid, collisional regime inhabited by tokamak edge plasmas, electrons can be nonadiabatic only when the turbulence can compete with this. But in a computation it is also necessary to retain coupling to parallel ion velocity fluctuations ($\tilde{u}_\parallel$), which at a large parallel gradient becomes effective, even though the ion dynamical rates are inherently much slower. As a result, part of the computational domain is deep into the adiabatic regime for electrons. What is needed is a computational method which can treat a ratio of parallel electron dynamics to turbulence and wave frequencies which can take arbitrarily large or small values: it must be stiffly stable. Further, since the questions whether drift waves are stable in the linear regime or whether strong turbulence will be present have rather subtle resolutions, the method must not introduce a large amount of spurious dissipation. Such a numerical method has already been published [1], and it is the basis for several computations of this dynamics in a two-dimensional sheared slab geometry [7–9]. However, being a purely implicit (backward Cauchy–Euler) method it is only first-order accurate in the time step, so the computations have been rather expensive. Since the validity of the results in two dimensions can be questioned, one would like to extend the computations to full toroidal geometry. Toroidal computations have begun, but present-day resources allow only inadequate [10] or marginal [11] resolution.

The purpose of this paper is to surmount this difficulty and facilitate the development of fully resolved computations in toroidal geometry in the near future. Recent computations using the implicit method have done so only for the parallel electron dynamics, leaving the remaining parts to be done with a second-order predictor–corrector scheme (second-order Runge–Kutta). This was adequate for the turbulence (which must be completely resolved temporally, anyway) and for the linear gradient terms, but it created problems in the studies involving sheared E $\times$ B flows. When sheared flows were present [9] it was necessary to reduce the time step by a factor of 3 below what is otherwise customary [7]. In this paper, the implicit method itself is extended to include the terms describing E $\times$ B advection, linear gradient forcing, and parallel ion dynamics, in addition to the parallel electron dynamics. Then, an existing stepping algorithm which is both second-order accurate and stiffly stable is applied to the present problem. Briefly, each time step is split into three segments: two implicit steps of equal length separated by an explicit (Eulerian extrapolation) step. The relative fractions of each are adjusted to match all terms in the corresponding Taylor expansion through second order [2]. The nonlinear terms (the turbulence) as well as smaller terms representing the effects of magnetic field gradient and curvature are treated with the predictor–corrector as before. The result is a new method which is both more accurate and faster than that used previously [1].

The following sections introduce the problem to be solved, detail the implicit part of the method and the stepping order, and provide tests showing the improvements in performance. Although the tests given here are done for linear waves and two-dimensional turbulence in slab geometry, the principle conclusion is that fully resolved computation in three dimensions is now available to those who can command significant fractions of the largest and fastest computers now in operation.

II. DEFINITION OF THE PROBLEM

The physical system and set of equations used herein have been completely detailed elsewhere [7]; a brief de-

scription follows. The physical milieu is electron fluid dynamics at drift scales. Dynamical rates (ω) are much slower than plasma (ω_p) or gyration frequencies (Ω) of either species, the electron collision frequency (ν_e) or magnetohydrodynamical (MHD) scales, but much faster than that of perpendicular dissipation via collisional exchange of gyro orbits. Spatial scales for the fluctuations (Δ) are smaller than those of the background quantities (L) but larger than the collisionless skin depth, Debye length, or gyroradii. In this regime, each species may be treated as a fluid with its own density and temperature, as was done by Braginskii [12]. Due to the slowness of ω, the plasma is quasineutral: ϕ does not vanish, but $n_i \approx n_e \equiv n$. This requires that $\omega \ll \Omega_i \ll \omega_{pi}$, which is easily satisfied by tokamak edge turbulence. One important limitation for this study is that the drift wave dispersion scale, $\rho_s = c(M_i T_e)^{1/2}/eB$, must be retained. Since this is the same size as the ion gyroradius in $T_i = T_e$, one is restricted to cold ions: $T_i \ll T \equiv T_e$. This being the case, the ions may still be treated as a fluid although the ion–ion collision frequency (as opposed to ν_e) is usually negligible for tokamak edge turbulence. Relaxation of this limit, using either "gyrofluid" [13] or gyrokinetic [14] approaches, is left to later work. With this caveat, the wide range of time and space scales experienced by the turbulence can be treated so long as all satisfy the above ordering, which is most often the case. As far as fluctuation levels are concerned, it is assumed that the relative amplitudes $e\tilde{\phi}/T$, $\tilde{n}/n$, $\tilde{T}/T$, are all commensurate with each other but small in the measure Δ/L.

Following Drake and Antonsen's nonlinear MHD treatment [15], the Braginskii equations [12] are reduced by solving for the electron and ion velocities perpendicular to the magnetic field:

$$\text{electrons: } \mathbf{v} = \mathbf{v}_E + \mathbf{v}_*, \tag{4}$$

$$\text{ions: } \mathbf{u} = \mathbf{v}_E + \mathbf{v}_p, \tag{5}$$

where the E × B velocity, $\mathbf{v}_E$, the diamagnetic drift, $\mathbf{v}_*$, and the polarisation drift, $\mathbf{v}_p$, are given by

$$\mathbf{v}_E = \frac{c}{B^2}\mathbf{B}\times\nabla_\perp\phi, \quad \mathbf{v}_* = -\frac{c}{neB^2}\mathbf{B}\times\nabla_\perp p, \quad \mathbf{v}_p = -\frac{M_i c^2}{eB^2}\frac{d}{dt}\nabla_\perp\phi, \tag{6}$$

respectively. The advective derivative appearing in $\mathbf{v}_p$ is with the E × B velocity,

$$\frac{d}{dt} = \frac{\partial}{\partial t} + \mathbf{v}_E\cdot\nabla, \tag{7}$$

due to the fact that $\mathbf{v}_p \ll \mathbf{v}_E$.

These perpendicular velocities are then substituted into the advection and divergence terms in the rest of the fluid equations. Because of the quasineutrality there is only one density equation, but both ion and electron divergences occur in the charge conservation equation, $\nabla\cdot\mathbf{J} = 0$. Parallel velocities are left as is, but the electron piece is eliminated in favor of $J_\parallel$, which satisfies a collisional Ohm's law determined by a balance between forces on the electrons and friction against the ions. In the process, two further assumptions are made: (a) The plasma pressure is low enough so that the field lines remain unperturbed and the motion is electrostatic. In the collisional regime this requires that the plasma beta satisfy $\beta L_s^2/L^2 \ll 1$, where L_s is the shear length of the magnetic field and L is the scale length of the dominant gradient, ∇n or ∇T [7, 16]. (b) The background plasma current is everywhere negligibly small, so that the effects of rippling instabilities do not enter. The condition for this is $(J/nec_s)(L/L_s) \ll 1$, where $c_s = (T_e/M_i)^{1/2}$ is the sound speed [17, 18]. In Langmuir probe experiments both conditions are satisfied easily. Additionally, terms which are formally small by Δ/L, e.g., parallel advection by $\tilde{u}_\parallel$, are strictly neglected. Due to these restrictions and the general drift ordering, the only nonlinear terms appearing in the equations are those involving advection by the E × B velocity; these are called "E × B nonlinearities."

Since the present purpose is to exemplify the computational method the geometry is simplified to the two-dimensional slab system used previously [7, 8]. The right-handed, orthonormal coordinate system (x, y, z) is locally field-aligned, with ∇z in the direction of $\mathbf{B}$ at a prescribed reference location, $x = 0$. The background ∇n and ∇T are in the direction of $-\nabla x$, leaving ∇y in the electron drift direction given by $\nabla p \times \mathbf{B}$. The magnetic field is

$$\mathbf{B} = B\left(\nabla z + \frac{x}{L_s}\nabla y\right),$$

with B and L_s constant. The ∇B terms are introduced by allowing B a slight gradient in the direction of $-\nabla x$, of scale length $L_B \gg L$. The background gradients are kept fixed, as is most appropriate in a treatment of 2D, localised turbulence [7]. In slab geometry the differential operators are

$$\frac{d}{dt} = \frac{\partial}{\partial t} + \frac{c}{B}\nabla z\cdot\nabla\phi\times\nabla, \tag{8}$$

$$\nabla_\parallel = \frac{x}{L_s}\frac{\partial}{\partial y}, \tag{9}$$

$$\nabla_\perp^2 = \frac{\partial^2}{\partial x^2} + \frac{\partial^2}{\partial y^2}, \tag{10}$$

noting the absence of $\mathbf{v}_*$ in (d/dt) due to the well-known

diamagnetic cancellation [19]. One should note that the second term on the right side of Eq. (8) contains the E × B nonlinearity, linear gradient forcing, and E × B shear flow advection. Below, these are separated. In Eqs. (9), (10), the subscripts "$\|$" and "$\perp$" denote the components parallel and perpendicular to the magnetic field, respectively.

The equations are normalised relative to the background at the reference flux surface, $x = 0$, also called the "resonant surface" since $\nabla_\|$ vanishes there. The reference time scale is c_s/L_n, and the spatial scale is ρ_s. The relative amplitudes scaled by the small parameter $\delta = \Delta/L_n$. Explicitly,

$$\phi \leftarrow \delta^{-1}\frac{e\tilde{\phi}}{T}, \quad n \leftarrow \delta^{-1}\frac{\tilde{n}}{n}, \quad T \leftarrow \delta^{-1}\frac{\tilde{T}}{T}, \quad u \leftarrow \delta^{-1}\frac{\tilde{u}_\|}{c_s}, \tag{11}$$

where quantities appearing without the tilde on the right side refer to the background at $x = 0$. In normalised units, the two scales ρ_s and c_s/L_n take the values of unity.

With all of the foregoing, the problem is defined as follows:

The four dependent variables, ϕ, n, T, and u, are defined on a two-dimensional spatial domain, Ω, given by $x \in [-x_L, x_L]$ and $y \in [0, 2\pi/K]$, where x_L and K are constant parameters. The temporal domain is $t > 0$. The four dependent variables are specified at $t = 0$ for all $(x, y) \in \Omega$. They are assumed to vanish for $x = \pm x_L$ and to be periodic in y, e.g., $\phi(x, 2\pi/K) = \phi(x, 0)$. Subject to these constraints, the four dependent variables satisfy the equations

$$\left[\frac{\partial}{\partial t} + \{\phi,\} + V_y(x)\frac{\partial}{\partial y}\right]\left(\frac{\partial^2}{\partial x^2} + \frac{\partial^2}{\partial y^2}\right) \times \phi = W_y(x)\frac{\partial \phi}{\partial y} + Dx^2\frac{\partial^2}{\partial y^2}(\hat{\alpha}T + n - \phi) - \omega_B\frac{\partial}{\partial y}(n + T), \tag{12}$$

$$\left[\frac{\partial}{\partial t} + \{\phi,\} + V_y(x)\frac{\partial}{\partial y}\right] \times n = -\omega_n\frac{\partial \phi}{\partial y} + Dx^2\frac{\partial^2}{\partial y^2}(\hat{\alpha}T + n - \phi) - \varepsilon x\frac{\partial u}{\partial y} - \omega_B\frac{\partial}{\partial y}(n + T - \phi), \tag{13}$$

$$\left[\frac{\partial}{\partial t} + \{\phi,\} + V_y(x)\frac{\partial}{\partial y}\right] \times T = -\omega_T\frac{\partial \phi}{\partial y} + \frac{2}{3}\hat{\alpha}Dx^2\frac{\partial^2}{\partial y^2}(\hat{\alpha}T + n - \phi) + \frac{2}{3}\kappa Dx^2\frac{\partial^2 T}{\partial y^2} - \frac{2}{3}\varepsilon x\frac{\partial u}{\partial y} - \frac{2}{3}\omega_B\frac{\partial}{\partial y}\left(n + \frac{7}{2}T - \phi\right), \tag{14}$$

$$\left[\frac{\partial}{\partial t} + \{\phi,\} + V_y(x)\frac{\partial}{\partial y}\right] \times u = -\omega_u\frac{\partial \phi}{\partial y} - \varepsilon x\frac{\partial}{\partial y}(n + T) + \mu_\| x^2\frac{\partial^2 u}{\partial y^2}, \tag{15}$$

where $\hat{\alpha} = 1.71$ and $\kappa = 1.6$ are constants, and ω_n, ω_T, ω_u, D, ε, $\mu_\|$, and ω_B are constant parameters, and $V_y(x)$ and $W_y(x)$ are specified functions. The second term on the left side of each equation is the E × B nonlinear advection term, e.g.,

$$\{\phi, n\} = \frac{\partial \phi}{\partial x}\frac{\partial n}{\partial y} - \frac{\partial n}{\partial x}\frac{\partial \phi}{\partial y}. \tag{16}$$

The term involving $\mu_\|$ is an artificial parallel viscosity which under the cold ion restriction takes the place ion Landau damping has when the ions are warm [7]. All constants, parameters, and variables as described in this paragraph are real.

The dependent variables are expressed in a Fourier representation, e.g.,

$$\phi(x, y) = \sum_{l=1}^{N} \phi_l e^{ik_y y} + \text{c.c.}, \quad k_y = lK, \tag{17}$$

where the subscript denotes the lth harmonic of the fundamental component and N is the number of complex components. In order to ensure de-aliasing, N is always one-third of a power of two, rounded down. In Fourier, or xk_y-space, the parallel gradient operator becomes a multiplying factor,

$$\nabla_\| \rightarrow ik_\| = ixk_y. \tag{18}$$

This greatly facilitates the development of an implicit algorithm. Transformation between xy- and xk_y-space proceeds through a standard fast Fourier transform. Because of the strong inhomogeneity in the x-direction (pure hydrodynamic to deep adiabatic conditions over a distance Δ_D which is usually less than the scale of ϕ) that direction is never transformed; derivatives in the x-direction are expressed through finite differences over a grid of M points, the first and last of which are at $x = \pm x_L$, respectively. A resolution function is specified,

$$x_L\frac{\partial f}{\partial x} = \frac{(1 - f_1)f_0}{\tanh f_0}\operatorname{sech}^2 f_0 x + f_1, \tag{19}$$

through which the interval $[-x_L, x_L]$ in x is mapped to the interval $[-1, 1]$ in f. Derivatives are expressed through the chain rule, so that centered differences are taken in the

equidistantly spaced f. This is simple because f is infinitely differentiable. In xk_y-space one has

$$\frac{\partial \phi}{\partial x}(x_i, l) = \frac{\phi_{i+1,l} - \phi_{i-1,l}}{2h} f'(x_i),$$
$$\nabla_\perp^2 \phi(x_i, l) = a_i \phi_{i-1,l} + d_{i,l}\phi_{i,l} + c_{i,l}\phi_{i+1,l}, \tag{20}$$

where $h = 2/(M-1)$ is the interval in f, the prime denotes $(\partial/\partial x)$, and the Laplacian matrix elements are

$$a_i = \frac{f''(x_i)}{h^2} - \frac{f'(x_i)}{2h}, \quad c_{i,l} = \frac{f''(x_i)}{h^2} + \frac{f'(x_i)}{2h},$$
$$d_{i,l} = -(a_i + c_i) - l^2 K^2. \tag{21}$$

The $c_{i,l}$'s depend on l because they are affected by the $d_{i,l}$'s in the triangularisation. The grid point locations, x_i, are obtained by integrating Eq. (19) numerically.

In turbulence computations only, an artificial dissipation term in the form of a small hyperviscosity, $\mu_\perp \nabla_\perp^4$, is added to the square brackets on the left side of each of Eqs. (12)–(15). The purpose is to contain the spectral transfer tendency towards small scales. In xk_y-space the hyperviscosity is a pentadiagonal matrix which is derived from the Laplacian matrix and the chain rule on the grid map in Eq. (19) by straightforward means.

In terms of the physics, the parameters in (12)–(15) are given by

$$D = \frac{c_s/L_n}{0.51\nu_e} \frac{M_i}{m_e} \frac{L_n^2}{L_s^2}, \tag{22}$$

$$\omega_n = 1, \quad \omega_T = L_n/L_T, \quad \omega_u = L_n/L_u, \tag{23}$$

$$\varepsilon = L_n/L_s, \quad K = k_0\rho_s, \quad \omega_B = 2L_n/L_B, \tag{24}$$

where the L's are the background scale lengths for the subscripted quantities, and $2\pi/k_0$ is the unnormalised periodicity length in the y-direction. The E × B shear flow $V_y(x)$ has been normalised to $(\rho_s c_s/L_n)$, and $W_y(x) = V_y''(x)$. Of the parameters, the most important is D, which gives the degree to which the electron dynamics will be adiabatic. In normalised units, adiabatic electrons means $n \to \phi$ and $T \to 0$. The ratio of linear gradient forcing to parallel collisional dissipation, taken at the lowest wavenumber k_0, gives the collisionality,

$$C = 0.51 \frac{\nu_e}{\omega_*} \frac{m_e}{M_i} \frac{L_s^2}{L_n^2} \equiv \frac{\Delta_D^2}{\rho_s^2}, \tag{25}$$

where $\omega_* = ck_0T/eBL_n$ is the diamagnetic frequency, and the second equality is used to define a new scale length, Δ_D. This is called the nonadiabatic, or hydrodynamic, layer width and represents the width of the region in which departures from adiabatic behaviour in the electrons are important. If $C > 1$, then the range of scales of motion excited in the turbulence ($\Delta \gtrsim \Delta_D$) are relatively nondispersive, and the drift wave turbulence exhibits a nonlinear instability: it is self-sustaining even though the corresponding linear waves are all damped [7, 8]. This result provides the motivation for continuing the development of numerical methods capable of treating high-resolution simulation of drift wave turbulence.

III. THE NUMERICAL STEPPING ALGORITHM

The basic scheme by which the linear terms (except those involving ω_B) in Eqs. (12)–(15) are solved is a three-segment stepping algorithm: an implicit (backward Cauchy–Euler) step is taken, followed by an explicit step (Eulerian extrapolation), followed by another implicit step [2]. The fraction of the total time step taken by each is adjusted such that all the terms in the temporal Taylor expansion through second order in the time step are recovered. As an example, consider the simple linear advection equation given by

$$\dot{F} = -i\alpha F, \tag{26}$$

where F is a complex function of the real variable t, α is a real parameter, and the dot refers to differentiation with respect to t. It is desired to find $F(t+\tau)$ given $F(t)$. Simple implicit and explicit steps may be respectively represented by

$$F(t+\tau) = \frac{F(t)}{(1 + i\tau\alpha)}, \quad F(t+\tau) = (1 - i\tau\alpha)F(t). \tag{27}$$

Both expressions satisfy the Taylor expansion,

$$F(t+\tau) = (1 - i\tau\alpha - \tfrac{1}{2}\tau^2\alpha^2 + \cdots)F(t), \tag{28}$$

only to first order. One could improve this by using the second-order predictor–corrector scheme,

$$F^* = (1 - \tfrac{1}{2}i\tau\alpha)F(t), \quad F(t+\tau) = F(t) - i\tau\alpha F^*, \tag{29}$$

but the benefit of stiff stability conferred by the implicit step would be lost. This is acceptable for the turbulence, complete resolution of which is desired, but not for the parallel electron dynamics or E × B shear flow advection, both of which inhabit regions of Ω where their corresponding physics do not really enter (at large $|x|$ and k_y the electrons are deeply adiabatic and the amplitudes of the localised fluctuations are negligibly small). One can, however, combine the two types of steps in Eq. (27) to retain both second-order accuracy and stiff stability:

$$F^{(1)} = \frac{F(t)}{(1 + i\theta_1\tau\alpha)}, \quad F^{(2)} = (1 - i\theta_2\tau\alpha)F^{(1)},$$
$$F(t + \tau) = \frac{F^{(2)}}{(1 + i\theta_3\tau\alpha)}, \tag{30}$$

in a routine known as DIRK2 [2]. The first term in Eq. (28) is matched by choosing the step functions, θ, to satisfy $\theta_1 + \theta_2 + \theta_3 = 1$. The second term in Eq. (28) is matched if $\theta_2^2 = \theta_1^2 + \theta_3^2$. These conditions are satisfied by the choice

$$\theta_1 = \theta_3 = \frac{1}{2 + \sqrt{2}}, \quad \theta_2 = \frac{\sqrt{2}}{2 + \sqrt{2}}. \tag{31}$$

Stiff stability results from there being two contributions of $\tau\alpha$ in the denominator of the amplification factor opposing only one in the numerator:

$$F(t + \tau) = \xi F(t), \quad \xi = \frac{(1 - i\theta_2\tau\alpha)}{(1 + i\theta_1\tau\alpha)(1 + i\theta_3\tau\alpha)}. \tag{32}$$

Further, one can verify by examination of $|\xi|^2$ that the amplitude of F (which in the exact solution does not change) is unaffected at second order (like the predictor–corrector) and damped at fourth order (where the predictor–corrector grows). These properties are exactly what one desires for the parallel electron dynamics and E × B shear flow advection in drift wave turbulence.

This simple algorithm must be applied to the drift wave system, Eqs. (12)–(15), and to do that one must develop an implicit step where as much of the work as possible is done analytically. That is, one would like to avoid block inversion techniques, since for drift wave dynamics these carry the danger that the rapid parallel dissipation manifests itself as spurious perpendicular diffusion in n and T caused by the $\nabla_\perp^2$ operator in Eq. (12). The technique used in an implicit step is to solve for u, T, and n in terms of ϕ, then to solve a tridiagonal matrix equation for ϕ, and then simply obtain n, T, and u. Because of the form of $\nabla_\parallel$, this can only be done in xk_y-space, which is what necessitates the Fourier representation. Up to now, the scheme which has been used by this author [7–9] treated only the parallel dissipation terms (those involving D) implicitly, leaving others to be done by predictor–corrector (turbulence and E × B shear flow) or simply explicitly (gradient forcing and magnetic curvature).

Such an implicit scheme has already been published, for the simplified drift wave system in which T is left out [1]. In the most basic form, the parallel electron dissipation involves relaxation to adiabatic behaviour of the linear system

$$\frac{\partial}{\partial t}\nabla_\perp^2\phi = -Dk_\parallel^2(n - \phi), \quad \frac{\partial n}{\partial t} = -Dk_\parallel^2(n - \phi), \tag{33}$$

where $k_\parallel^2 = x^2k_y^2$ is a real variable in Fourier representation. This is differenced in time so that

$$\nabla_\perp^2\phi = \nabla_\perp^2\phi^{(0)} - \alpha(n - \phi), \quad n = n^{(0)} - \alpha(n - \phi), \tag{34}$$

where $\alpha = \tau Dk_\parallel^2$ and the superscript denotes values at the backward time step. One solves the second expression in Eq. (34) for n in terms of ϕ and then substitutes into the first, yielding the implicit stepping scheme:

$$\left(\nabla_\perp^2 - \frac{\alpha}{1 + \alpha}\right)\phi = \nabla_\perp^2\phi^{(0)}, \quad n = \frac{n^{(0)} + \alpha\phi}{1 + \alpha}. \tag{35}$$

The operator acting on ϕ in Eq. (35) is a tridiagonal matrix similar to that in Eq. (20); this is solved to obtain ϕ, which is then substituted into the second expression in Eq. (35) to obtain n. It was shown previously [1] that the eigenvalues of the corresponding amplification matrix are both unity when $\alpha = 0$, and in the limit $\alpha \to \infty$ one approaches zero and the other, unity. This means that in the adiabatic limit there is no spurious dissipation; the two eigenvalues correspond to the damping of $(n - \phi)$ and the lack of dissipation of $(n - \nabla_\perp^2\phi)$, respectively. When the electrons are asymptotically adiabatic, their parallel motion ceases to be an effective dissipation mechanism, and the quantity $(1 - \nabla_\perp^2)\phi$ becomes an invariant, up to other dissipation channels in the ion dynamics [20]. What inaccuracy there is in this scheme lies in the approach to adiabaticity, most important where $Dk_\parallel^2 \sim \omega$, or $x \sim C^{1/2}$ in normalised units. Too large a time step would result in overestimating how adiabatic the electrons are. The first-order accuracy results in the limitation of the time step experienced before [1].

For the implicit parts of the overall step in the DIRK2 scheme, this method is used not only for the parallel dissipation terms but also for those involving E × B shear flow advection, linear gradient forcing, and parallel ion motion. The last two might not be necessary, but since the E × B advection already involves all four dependent variables, those terms are easily included in the scheme. Only the ω_B terms are left out. On the one hand, they are even slower than the linear gradient forcing terms; on the other, in many geometries they involve derivatives in the x-direction, and, except for the $\nabla_\perp^2$ operator in Eq. (12), this is to be avoided, as already explained. First, u, T, and n are eliminated in order to get the tridiagonal matrix equation for ϕ, and then the rest proceeds as a generalisation of Eqs. (34), (35). Considering all the linear terms, except those involving ω_B, one is given $\phi^{(0)}$, $n^{(0)}$, $T^{(0)}$, and $u^{(0)}$. One finds

$$u = S_u - A_{up}\phi - A_{uh}(n - \phi) - A_{ut}T,$$
$$T = S_t - A_{tp}\phi - A_{th}(n - \phi), \tag{36}$$
$$n - \phi = X_n(S_n - A_{hp}\phi),$$

where

$$\begin{aligned} S_u &= X_u u^{(0)}, \\ S_t &= X_t[T^{(0)} - \tfrac{2}{3} i\tau\varepsilon k_\parallel S_u], \\ S_n &= n^{(0)} - (\tau\hat{\alpha} D k_\parallel^2 - i\tau\varepsilon k_\parallel A_{uh}) S_t - i\tau\varepsilon k_\parallel S_u, \end{aligned} \tag{37}$$

and

$$\begin{aligned} X_u &= (1 + i\tau k_y V_y + \tau\mu_\parallel k_\parallel^2)^{-1}, \\ X_t &= [1 + i\tau k_y V_y + \tfrac{2}{3}\tau(\hat{\alpha}^2 + \kappa) D k_\parallel^2 - \tfrac{2}{3} i\tau\varepsilon k_\parallel A_{uh}]^{-1}, \\ X_n &= (1 + i\tau k_y V_y + x_n^2)^{-1}, \\ A_{up} &= A_{ut} = A_{uh} = i\tau\varepsilon k_\parallel X_u, \\ A_{tp} &= X_t(i\tau\omega_T - \tfrac{2}{3} i\tau\varepsilon k_\parallel A_{up}), \\ A_{th} &= \tfrac{2}{3} X_t(\tau\hat{\alpha} D k_\parallel^2 - i\tau\varepsilon k_\parallel A_{uh}), \\ A_{hp} &= 1 + i\tau k_y V_y + i\tau\omega_n - \tau\hat{\alpha} D k_\parallel^2 A_{tp} \\ &\quad - i\tau\varepsilon k_\parallel (A_{up} - A_{uh} A_{tp}), \\ x_n^2 &= \tau D k_\parallel^2 (1 - \hat{\alpha} A_{th}) - i\tau\varepsilon k_\parallel A_{uh}(1 - A_{th}). \end{aligned} \tag{38}$$

With this information, the equation to be solved for ϕ is given by

$$A_{p1} \nabla_\perp^2 \phi - A_{p2} \phi = S_p, \tag{39}$$

where

$$\begin{aligned} S_p &= \nabla_\perp^2 \phi^{(0)} - X_n x_n^2 S_n - \tau\hat{\alpha} D k_\parallel^2 S_t, \\ A_{p1} &= 1 + i\tau k_y V_y, \\ A_{p2} &= X_n x_n^2 A_{hp} + \tau\hat{\alpha} D k_\parallel^2 A_{tp} + i\tau W_y. \end{aligned} \tag{40}$$

This yields the tridiagonal matrix equation for ϕ; at each x_i Eq. (39) becomes

$$(a2)_{i,l} \phi_{i-1,l} + (d2)_{i,l} \phi_{i,l} + (c2)_{i,l} \phi_{i+1,l} = (S_p)_{i,l}, \tag{41}$$

where

$$(a2)_{i,l} = A_{p1} a_i, \quad (c2)_{i,l} = A_{p1} c_{i,l}, \quad (d2)_{i,l} = A_{p1} d_{i,l} - A_{p2}, \tag{42}$$

with a_i, $d_{i,l}$, and $c_{i,l}$ given in Eq. (21). Once Eq. (41) is solved to obtain ϕ, the other dependent variables are obtained from Eqs. (36). The auxiliary variable, $\nabla_\perp^2 \phi$, the E × B vorticity, is obtained by solving Eq. (39) directly for it, not by operation with the $\nabla_\perp^2$ matrix. This completes the implicit step. The reader may verify that it possesses the same desirable properties—amplification eigenvalues in the limits of large and small $\tau D k_\parallel^2$—as it does in the simpler, isothermal system as outlined above and before [1].

The entire algorithm for the full, nonlinear system in Eqs. (12)–(15) then proceeds as follows: (i) One starts with ϕ, n, T, u, and $\nabla_\perp^2 \phi$ at time t. (ii) The nonlinear and ω_B terms are advanced with the predictor–corrector scheme. In each segment thereof, the dependent variables are transformed to xy-space, terms involving $\{\phi, \}$ are computed and transformed back to xk_y-space, and the ω_B terms are added. After the first segment the intermediate quantity ϕ^* is computed from the intermediate vorticity using Eq. (20). After the second segment one has the four quantities n, T, u, and $\nabla_\perp^2 \phi$ updated by the $\{\phi, \}$ and ω_B terms. (iii) Artificial dissipation is applied to each of these to obtain $n^{(0)}$, $T^{(0)}$, $u^{(0)}$, and $\nabla_\perp^2 \phi^{(0)}$. (iv) An implicit step is taken using Eqs. (36)–(42) with a partial time step of $\theta_1 \tau$, obtaining the intermediate quantities $\phi^{(1)}$, $n^{(1)}$, $T^{(1)}$, $u^{(1)}$, and $\nabla_\perp^2 \phi^{(1)}$. (v) An explicit step is taken by evaluating the linear terms (except ω_B) using the quantities superscripted by "(1)," and then taking the linear extrapolation over the partial time step $\theta_2 \tau$. One now has the intermediate quantities $n^{(2)}$, $T^{(2)}$, $u^{(2)}$, and $\nabla_\perp^2 \phi^{(2)}$. (vi) Another implicit step is taken with a partial time step of $\theta_3 \tau$. With all dependent variables in hand at time $t + \tau$, the step is complete.

IV. NUMERICAL TESTS

In this section, tests of the accuracy of the time-stepping algorithm are presented. Tests of spatial resolution have been performed elsewhere [1, 7]; this is neglected here on the grounds that the previous algorithm has already correctly represented the physics of Eqs. (12)–(15). Testing is done on two schemes: DIRK2, the new one presented herein, and IMPL ($k_\parallel$ terms first-order implicit; others explicit), which is the old one [1] generalised to incorporate T.

In the diagnosis of the numerical performance of the two schemes, the energy theorem for Eqs. (12)–(15) is used [7]: One defines the fluctuation-free energy,

$$E = \tfrac{1}{2} \langle (|\nabla_\perp \phi|^2 + |n|^2 + \tfrac{3}{2}|T|^2 + |u|^2) \rangle, \tag{43}$$

and then notes that E evolves according to Eqs. (12)–(15) as

$$\frac{1}{2E} \frac{\partial E}{\partial t} \equiv \Gamma, \quad \Gamma - (\Gamma_t + \Gamma_n - \Gamma_c - \Gamma_k - \Gamma_s) = \Gamma_E, \tag{44}$$

where the source/sink rates are given by

$$
\begin{aligned}
2E\Gamma_n &= \langle nv_x\rangle,\\
2E\Gamma_t &= \tfrac{3}{2}\eta_e\langle Tv_x\rangle,\\
2E\Gamma_c &= D\langle|\nabla_\parallel(\hat{\alpha}T + n - \phi|^2\rangle,\\
2E\Gamma_k &= \kappa D\langle|\nabla_\parallel T|^2\rangle,\\
2E\Gamma_s &= \mu_\parallel\langle|\nabla_\parallel u|^2\rangle,
\end{aligned}
\tag{45}
$$

where $v_x = -\partial\phi/\partial y$ and Γ_E gives the error. The angle brackets denote integration over the two-dimensional domain, Ω. For a single k_y-component, as in the case of a localised linear wave, they reduce to an integration over x, replacing, e.g., nv_x with 2 Re n^*v_x in Γ_n. In case (A), below, each contribution to E reduces to a squared amplitude and each source/sink term to a simple product, e.g., $\Gamma_n \to$ Re n^*v_x/E. The symbol Γ is used to denote a time-dependent amplitude growth rate; the symbol γ is reserved for the growth rate of the linear eigenfunction.

This section is divided into three subsections: (A) Comparison of the DIRK2 and IMPL schemes to the exact solution for linear waves in a shearless slab with a finite parallel gradient, retaining only the background plasma gradients and the parallel electron dynamics. (B) Comparison of the DIRK2 and IMPL schemes for linear, localised waves in a sheared slab, with and without magnetic field inhomogeneity and without E × B flow shear. (C) Comparison of the DIRK2 and IMPL schemes for two-dimensional turbulence in a sheared slab, with all the terms present.

A. *Linear Waves, Shearless Slab*

The subset of Eqs. (12)–(15) treated in this subsection may be represented in matrix form:

$$\dot{\mathbf{u}} = \mathbf{A}\cdot\mathbf{u}, \tag{46}$$

where

$$
\mathbf{u} = \begin{pmatrix}\phi\\ n\\ T\end{pmatrix},
$$

$$
\mathbf{A} = \begin{pmatrix}
-Dk_\parallel^2/k^2 & Dk_\parallel^2/k^2 & \hat{\alpha}Dk_\parallel^2/k^2\\
-ik_y\omega_n + Dk_\parallel^2 & -Dk_\parallel^2 & -\hat{\alpha}Dk_\parallel^2\\
-ik_y\omega_T + \tfrac{2}{3}\hat{\alpha}Dk_\parallel^2 & -\tfrac{2}{3}\hat{\alpha}Dk_\parallel^2 & -\tfrac{2}{3}(\hat{\alpha}^2+\kappa)Dk_\parallel^2
\end{pmatrix},
\tag{47}
$$

with $k_\parallel$ a constant, representative value for xk_y, and $k = k_y$ (k_x ignored). Both $\mathbf{u}$ and $\mathbf{A}$ are complex. Eqs. (46), (47) can be solved to find the exact solution for the initial-value problem. Here, this is not done since the present purpose is served by finding the largest eigenvalue of $\mathbf{A}$ for comparison to the numerical results at a large time interval away from the start (the decaying transients are very fast, and it is not necessary to track them).

The two schemes were tested against each other and against the exact solution for one representative case. The parameters were chosen as follows: $Dk_\parallel^2 = 3.0$, $k = k_y = 0.5$, $\omega_n = 1$, and $\omega_T = 0.2$. The numerical constants were, as usual, $\hat{\alpha} = 1.71$ and $\kappa = 1.6$. For these parameters the largest eigenvalue of $\mathbf{A}$ is given by *Mathematica* as $\gamma - i\omega = 0.0127267 - i0.398368$, corresponding to a frequency of ω and a growth rate of γ. The values of τ used ranged from 10^{-2} to 10, cycling through a list of mantissas given by $\{1.0, 1.5, 2.0, 3.0, 5.0, 7.0\}$. The computations were carried out as follows: At $t = 0$ the dependent variables were set to $\phi = n = 10^{-8}$ and $T = 0$. Every $\Delta t = {}_{\max}(0.1, \tau)$, to the nearest step, E and its contributions were taken, along with the phase, $-\arg\phi$. The run was carried to $t = 1000$, after which the values of γ and $\omega = -d(\arg\phi)/dt$ were measured as centered differences and averaged over $970 < t < 1000$. It was checked that the γ of each dependent variable was equal to the γ of E to at least the fourth decimal place. The results appear in Fig. 1. The IMPL scheme is stiffly stable, but loses accuracy quickly since it is only accurate to first order in τ. The DIRK2 scheme retains sharp convergence until $\tau Dk_\parallel^2 \gtrsim 1$. At the lower values, $\tau < 10^{-1}$, to which the IMPL scheme's usefulness is limited, the DIRK2 scheme differs from the exact solution in the fifth decimal place (exactly how much depends on where in the run the results are measured). The accuracy of the two schemes is shown by the dependence of each scheme's Γ_E as a function of τ: the IMPL scheme is accurate to first order and DIRK2 to second (for $\Gamma_E < 10^{-6}$ machine accuracy is a factor).

A further comparison was done between the DIRK2 scheme and the exact solution for various values of $Dk_\parallel^2$ at a given value of $\tau = 10^{-1}$. Figure 2 shows the numerical results, along with the relative error to the exact solution; e.g., for the growth rate, γ, the relative error to the exact γ_e is $\delta\gamma/\gamma = |\gamma - \gamma_e|/\gamma_e$. The high accuracy is evident; it is what would be expected from the result in Fig. 1 for $\tau = 10^{-1}$. This test ensures that the good behaviour of the DIRK2 scheme holds for essentially arbitrary $Dk_\parallel^2$. Not only are the results of the DIRK2 scheme convergent with each other, but they obey the exact solution to high precision.

B. *Linear Waves in a Sheared Magnetic Field*

Here, no exact solution is available, but the results of the last subsection give one confidence that highly convergent results are most likely also the correct ones. The set of equations solved numerically was that of Eqs. (12)–(15) without the terms involving $\{\phi, \}$, $V_y(x)$, or $W_y(x)$. In xk_y-space, each dependent variable is a complex function of x

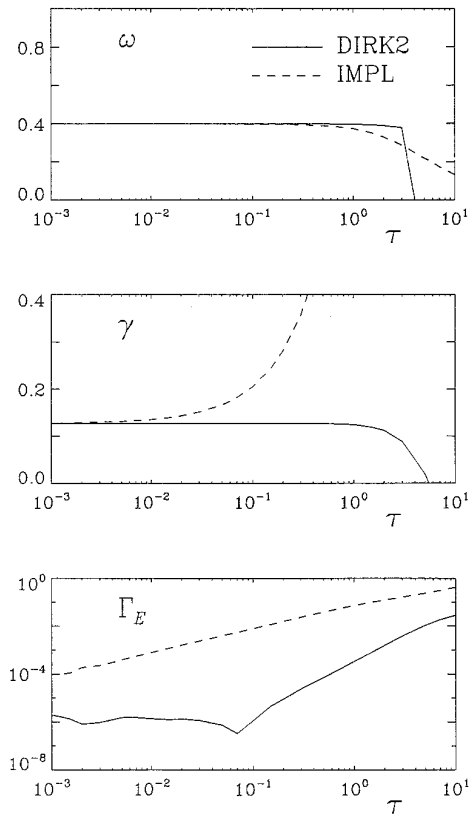

FIG. 1. Conversion of the DIRK2 and IMPL schemes against time step, τ, for a local, linear wave with $Dk_\parallel^2 = 3$, $K = 0.5$, and $\eta_e = 0.2$. Mode frequency (ω) and growth rate (γ) are better converged by the DIRK2 scheme. The energy error (Γ_E) reflects first-order convergence in the IMPL scheme and second-order in DIRK2.

(the subscript l is dropped for these linear runs), for $x \in [-x_L, x_L]$. The computations were set up much the same way as in the last subsection; at $t = 0$ the form of $\phi(x)$ was set to a special Gaussian: $\phi(x) = n(x) = 10^{-8} \exp(-x^2/\Delta^2)$, with $\Delta = 6$, and $T = u = 0$. The values of the source/sink terms were taken in the same way as before; Γ and Γ_E were measured at the end. The phase of ϕ was taken at $x = 0$. Each run was carried to $t = 300$, with measurements averaged over $270 < t < 300$.

For the first test ω_B was set to zero, and the other parameters were $D = 2.0$, $\varepsilon = 0.1$, $K = 0.3$, $\omega_n = \omega_T = 1$, $\mu_\parallel = 0.04$, and x_L was 20. Since these linear waves are always damped [16], an external drive term was added to Eq. (13), multiplying ω_n by $(1 + i\gamma_d)$, with $\delta_d = 0.3$. The source term Γ_n was changed accordingly. The same pattern of τ variation was taken as in the last subsection, but the range was $0.003 < \tau < 3.0$. The results for γ, ω, and Γ_E, shown in Fig. 3, show by the similarity to Fig. 1 that the behaviour of the two schemes is not changed by the introduction of magnetic shear and spatial structure. The sharp convergence of the DIRK2 scheme is maintained for $\tau < 1.0$. The IMPL scheme is restricted to $\tau \lesssim 5 \times 10^{-3}$. Finally, the run of $\Gamma_E(\tau)$ reflects the first- and second-order accuracy of the IMPL and DIRK2 schemes, respectively.

It is interesting to see what happens when the ω_B terms are introduced, since these are not part of the scheme by which parallel electron dynamics are treated. This introduces operator splitting, which means that the overall scheme will have first-order error scaling. Hence the need for this additional test: the external drive is dropped, and ω_B is set to 0.1, high enough to ensure the presence of a linear instability. Other than this exchange of ω_B for γ_d, this test was carried out identically to the one in Fig. 3. The results, shown in Fig. 4, indicate that although sharp convergence is still seen for $\tau \lesssim 1$, the error Γ_E is larger for the DIRK2 than for the IMPL scheme, and it shows first-order scaling as well. Although both the predictor–corrector for the ω_B terms and the DIRK2 scheme for the others are both second-order accurate, their split into separate operations is not. Nevertheless, that convergence extends to larger τ than for the IMPL scheme reflects the fact that the parallel electron dynamics itself is more accurately treated than in the IMPL scheme. It also reflects the slowness of the physics represented by the Ω_B terms. This experience shows that a low measured error in the energy is not a sufficient test of numerical performance, a lesson which is useful to other problems as well [21]. In this case, while the measured Γ_E for the IMPL scheme is

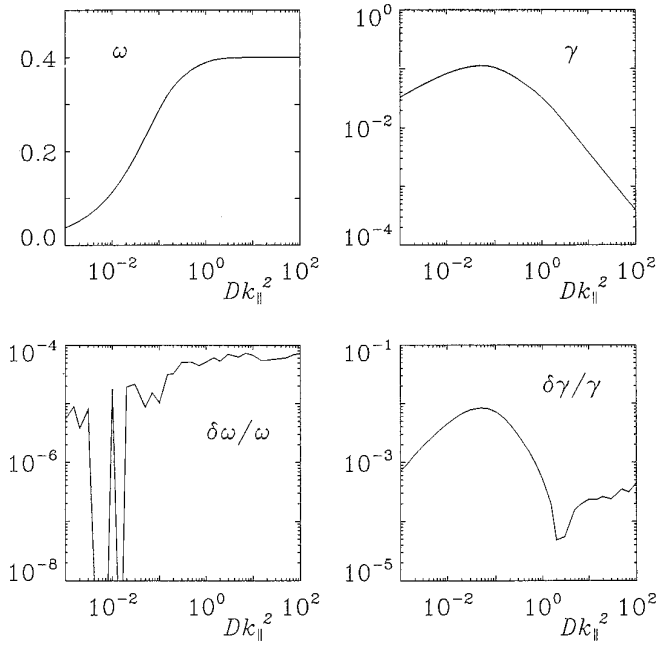

FIG. 2. Comparison of the DIRK2 scheme to the exact solution for $\tau = 10^{-1}$ for local, linear waves with $K = 0.5$ and $\eta_e = 0.2$, with $Dk_\parallel^2$ between 10^{-3} and 10^2. Mode frequency (ω) and growth rate (γ) from DIRK2 are shown along with the relative errors to the exact solution.

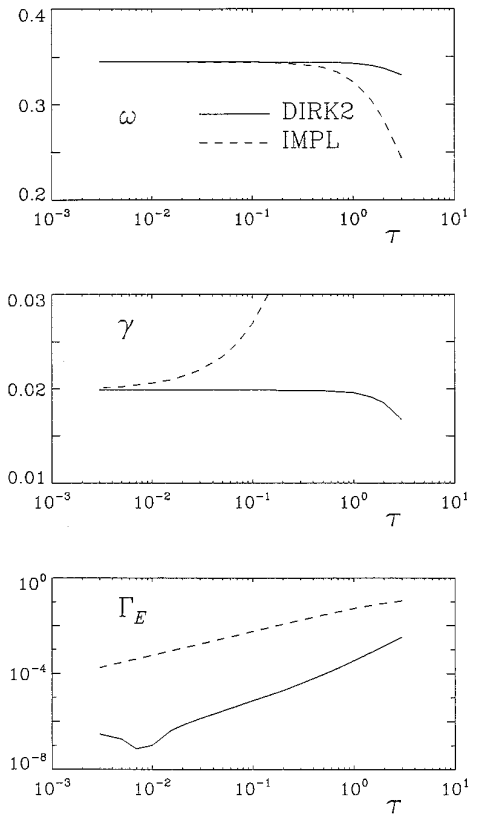

FIG. 3. Convergence of the DIRK2 and IMPL schemes against time step, τ, for a linear wave in a sheared-slab magnetic field with $Dk_\parallel^2 = 2$, $K = 0.3$, $\eta_e = 1.0$, and $\varepsilon = 0.1$, driven externally with $\gamma_d = 0.3$. Mode frequency (ω) and growth rate (γ) are better converged by the DIRK2 scheme. The energy error (Γ_E) reflects first-order convergence in the IMPL scheme and second-order in DIRK2; without the ω_B terms there is no operator splitting.

low, the loss of convergence for $\tau > 10^{-1}$ shows that mode structure errors are entering, which have a cancelling effect on the energy theorem. In addition to energy conservation, numerical schemes must also pass direct tests of convergence. So although the DIRK2 scheme has the higher Γ_E, it is still outperforming the IMPL scheme.

C. *Turbulence*

Here, the complete system, Eqs. (12)–(15), was evolved from an initial state characterised by adiabatic electrons and random relative phases [7]. The form of $\phi(x, y)$ at $t = 0$ was

$$\phi(x, y) = \exp(-x^2/\Delta^2)\Phi(x, y), \tag{48}$$

where again $\Delta = 6$, and Φ is a homogeneous, random-phase field given by

$$\Phi(x, y) = \sum_{k_x, l=1}^{N} A(k) \exp(ilKy + i\pi k_x x/x_L + i\Theta), \tag{49}$$

where Θ is a random variable on the interval $(0, 2\pi)$, the initial amplitude spectrum is

$$A(k) = (k/10)^{-1}[1 + (k/10)^4]^{-1/2}, \tag{50}$$

and $k = \sqrt{l^2K^2 + k_x^2}$. The initial amplitude was chosen to be $a_0 = 2.0$, with $\phi(x, y)$ rescaled such that

$$a_0 = 2\sum_{l=1}^{N} \int_{-x_L}^{x_L} dx\, |\phi_l(x)|^2. \tag{51}$$

The other dependent variables were set to $n = \phi$, and $T = u = 0$.

A reference run was set up and run to a point at which the whole of the mode structure—spectra of the E and Γ

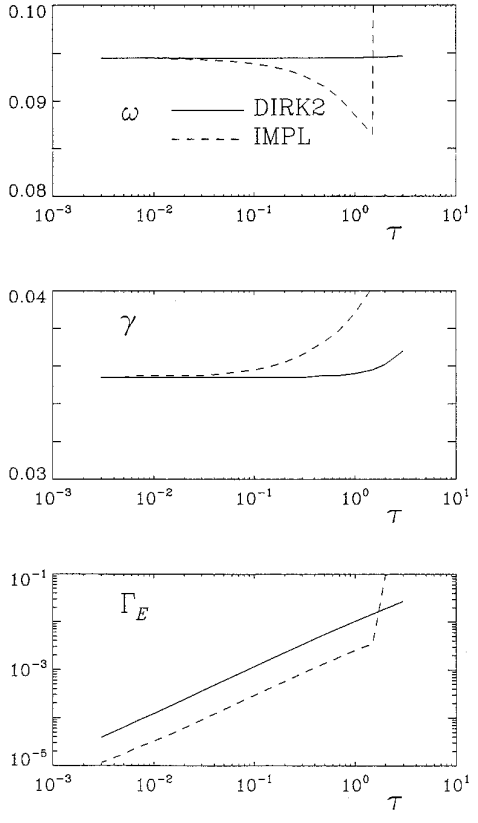

FIG. 4. Convergence of the DIRK2 and IMPL schemes against time step, τ, for a linear wave in a sheared-slab magnetic field with $Dk_\parallel^2 = 2$, $K = 0.3$, $\eta_e = 1.0$, and $\varepsilon = 0.1$, with magnetic field gradient $\omega_B = 0.1$. Mode frequency (ω) and growth rate (γ) are still better converged by the DIRK2 scheme. The energy error (Γ_E) now reflects first-order convergence in both schemes, because of the operator splitting in the DIRK2 scheme.

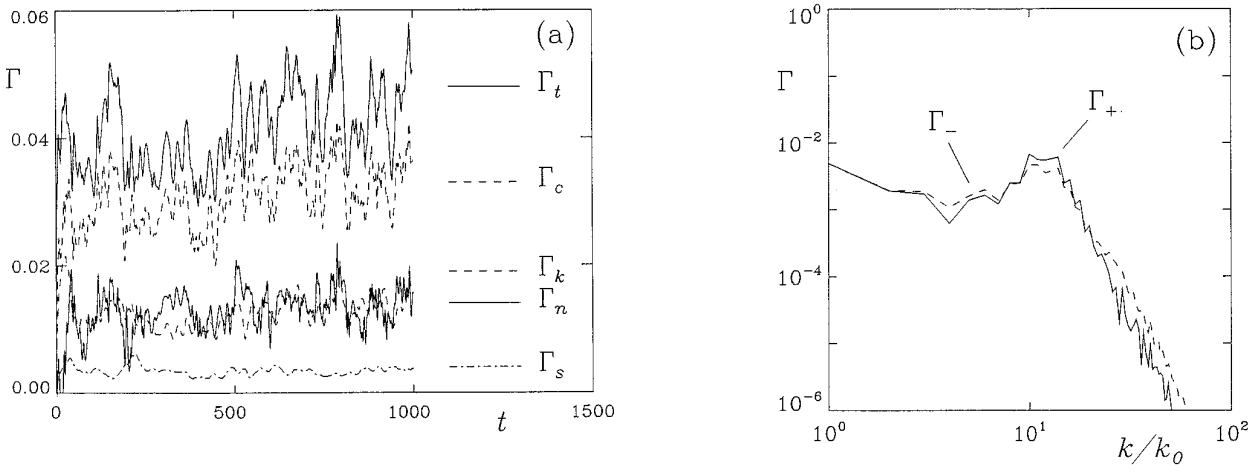

FIG. 5. Evolution of the source/sink terms (a) and spectra of the total sources and sinks (b), for the baseline run of turbulence in a sheared-slab magnetic field with $D = 4$, $K = 0.07$, $\eta_e = 1$, $\varepsilon = 0.07$, $\mu_\parallel = 0.04$, and $\mu_\perp = 3 \times 10^{-4}$. This is the basic nonlinear instability of collisional drift wave turbulence in a sheared magnetic field [7, 8].

terms, profiles of the Γ terms, and spectra of the mode widths of the fluctuations—is statistically stationary (see [7, Appendix B]). Parameters were $D = 4.0$, $\varepsilon = 0.07$, $K = 0.07$, $\omega_n = \omega_T = 1$, $\mu_\parallel = 0.04$, $\mu_\perp = 3 \times 10^{-4}$, and x_L was 20. The E × B shear and magnetic curvature terms were set to zero: $V_y = W_y = \omega_B = 0$. The number of Fourier harmonics of k_0 was 85. The number of grid points in the x-direction was 129, with grid parameters taking the values $f_0 = 4.0$ and $f_1 = 0.3$. The time step was $\tau = 0.1$. The run was carried to $t = 1000$, the starting point for the tests described below. The development of the Γ's and their spectra over the interval $750 < t < 1000$ are shown in Fig. 5. In this and all other respects, the results of Refs. [7, 8] are qualitatively reproduced by this run.

The first test was to check the convergence of the DIRK2 and IMPL schemes in the absence of E × B shear, both with respect to the time step and against each other. Parameters were as in the reference run, with the addition of $\omega_B = 0.1$. For the DIRK2 scheme, the values of τ were 0.01 and 0.1; for the IMPL scheme they were 0.01, 0.03, and 0.1. Each test was carried roughly to $t = 1025$, allowing for some unevenness due to the use of exact values, e.g., $\tau = 0.07$. The evolution of Γ and Γ_E of these cases is shown in Fig. 6. Here, the actual dissipation by the hyperviscosity, Γ_r, was computed and added to the right side of Eq. (44), so that Γ_E is the actual error of the scheme (in other papers Γ_r is counted as part of Γ_E [7, 8, 9]). Figure 6 shows sharp convergence for the DIRK2 scheme; the Γ curves are nearly coincidental. As previously [1], the IMPL scheme performs well for $\tau = 0.01$ (corresponding to 0.001 for the normalisation and parameters of the case studied then) but badly for larger values. During the present tests, it has been observed that the DIRK2 scheme for $\tau = 0.1$ is faster on a Cray-YMP than the IMPL scheme for $\tau = 0.01$ by a

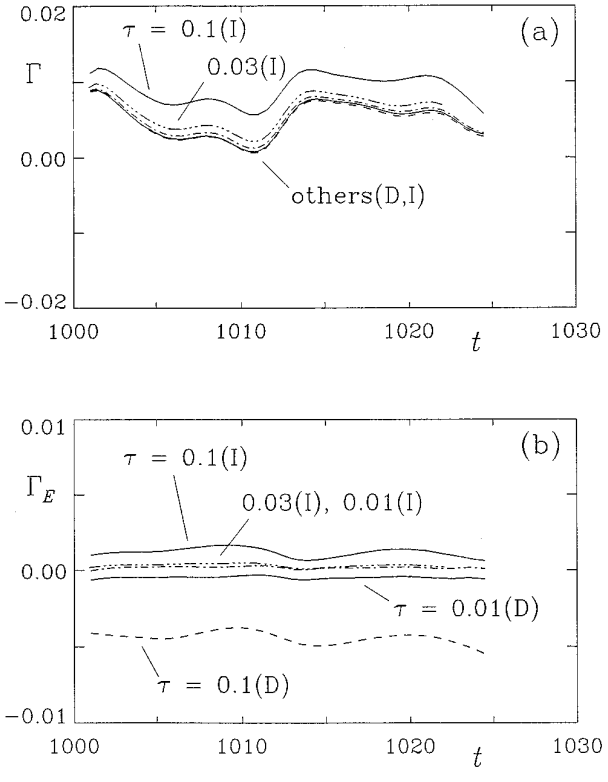

FIG. 6. Convergence of the DIRK2 and IMPL schemes against time step, τ, for the baseline run from Fig. 5, with the addition of $\Omega_B = 0.1$. The time step values used are given in the text. The overall growth rate comparison (a) shows good performance up to $\tau = 0.1$ for the DIRK2 scheme and the usual deterioration with $\tau > 0.01$ for the IMPL scheme [1]. The energy error (b) is increasingly excited with $\tau = 0.1$ for the DIRK2 scheme, but it is still small compared to the collisional sink rate, Γ_-.

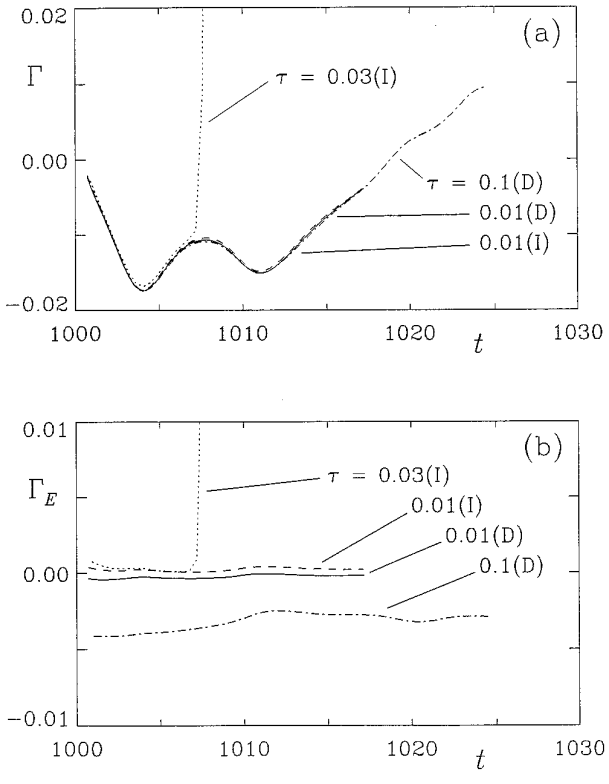

FIG. 7. Convergence of the DIRK2 and IMPL schemes against time step, τ, for the baseline run from Fig. 5, with the addition of the sheared E × B flow, $V = 0.3$. The time step values used are given in the text. The overall growth rate comparison (a) shows good performance up to $\tau = 0.1$ for the DIRK2 scheme, while the IMPL scheme can run only for $\tau = 0.01$ and smaller. The energy error (b) is increasingly excited with $\tau = 0.1$ for the DIRK2 scheme, but it is still small compared to the collisional sink rate, Γ_{-}.

factor of about 7. A similar test with $\omega_B = 0$ was also run, with the same results.

Before the final tests will all the terms, the two schemes were tested with the presence of an E × B flow with constant shear,

$$V_y(x) = Vx, \quad V = 0.3, \tag{52}$$

with $\omega_B = 0$ and other parameters as in the reference run. The two time steps, $\tau = 0.01$ and 0.1, were used for the DIRK2 scheme, and the values 0.01 and 0.03 were used for the IMPL scheme. In the IMPL scheme the predictor–corrector scheme used on the E × B shear terms limits τ drastically; the largest value of $V_y k_y$ is 35.7. This is enough to cause instability for $\tau = 0.03$, as shown in Fig. 7. With the E × B shear terms integral to the treatment of the parallel dissipation terms in the DIRK2 scheme, the larger value $\tau = 0.1$ was well-convergent with the lower values.

For the final test, solely on the performance of the DIRK2 scheme, the E × B shear terms were given the form

$$V_y(x) = Vx + \tfrac{1}{2}Wx^2, \quad W_y(x) = W, \tag{53}$$

with the constant parameters set to $V = 0.3$ and $W = 0.1$. Moreover, ω_B was set to 0.1. All terms in Eqs. (12)–(15) were now present. The values for τ ranged from 0.01 to 0.3, with the same mantissa set as in the linear tests. Overall convergence is shown in Fig. 8, with the same small differences in Γ as before. The nonlinear stability limit is finally reached with $\tau = 0.3$; up to that point the results are "reasonably convergent." What this means is (1) is the size of Γ_E is less than Γ_c or Γ_k and (2) variations in Γ_c (the one with the largest variation with τ) were of order a few percentages over a coherence time. Precisely, for $\tau = 0.01$, Γ_c was 0.0386 averaged between $1010 < t < 1020$, and for $\tau = 0.1$ it was 0.0368, both sampled 25 times. The coherence time is defined as the $1/e$ half-width of the envelope of the autocorrelation function; in this case using the envelope is important, due to the long-wavelength coherence [7]. The autocorrelation function was measured using a time series of $n(x = 0, y = 0)$, sampled

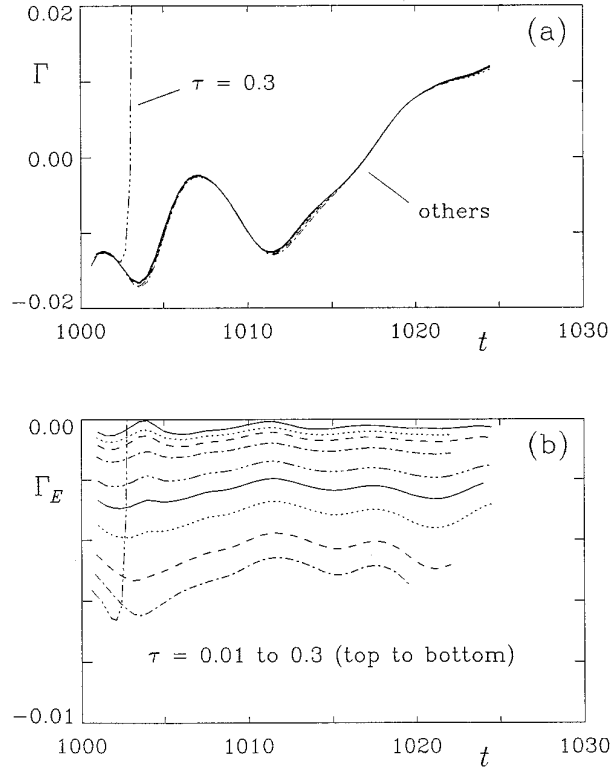

FIG. 8. Convergence of the DIRK2 scheme against time step, τ, for the baseline run from Fig. 5, with the addition of the sheared E × B flow, $V = 0.3$ and $W = 0.1$, and with $\omega_B = 0.1$; all terms present. The time step values used are given in the text. The overall growth rate comparison (a) shows good performance up to the nonlinear stability limit at $\tau = 0.2$. The energy error (b) is increasingly excited with $\tau = 0.1$ for the DIRK2 scheme, but it is still small compared to the collisional sink rate, Γ_{-}.

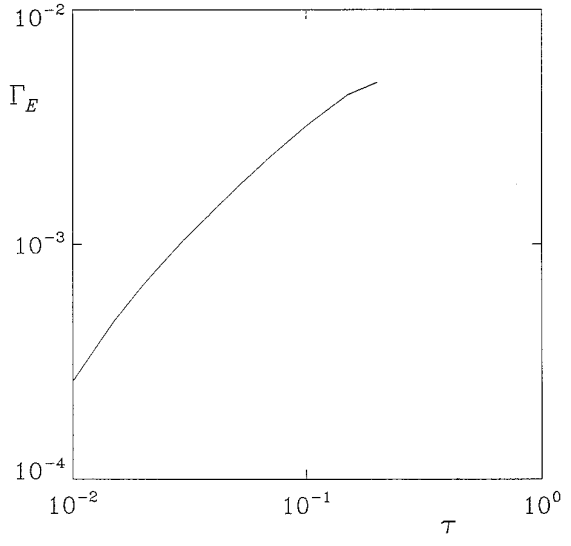

FIG. 9. Energy error, Γ_E, as a function of τ for the cases shown in Fig. 8 (except for the pathological $\tau = 0.3$). The closeness to a slope of $\Gamma_E \propto \tau$ reflects the operator splitting in the DIRK2 scheme.

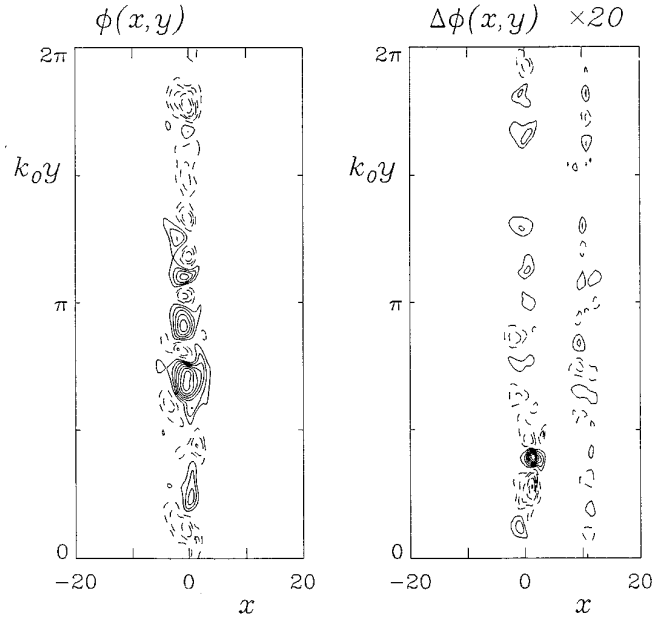

FIG. 11. Contours of $\phi(x, y)$ for the case $\tau = 0.01$ from Fig. 8, at $t = 1025$. The difference, $\Delta\phi$, is the result for the case $\tau = 0.1$, minus that for $\tau = 0.01$. The degree of nonconvergence is about 5% over a correlation time. The asymmetry is due to the presence of the E × B flow shear. The contour interval in both frames is 0.25.

every $\delta t = 0.5$ between $750 < t < 1000$, and the coherence time was estimated as $T_c = 25$. The average Γ_E is given as a function of τ in Fig. 9; the proportionality to τ is reflective of the first-order accuracy inherent in operator splitting, as in the case linear waves.

This convergence is illustrated as well in spectra and contours. These comparisons were done slightly differently; no measurements for Γ were taken, and the values of τ were adjusted slightly to ensure that all cases were compared at the same $t = 1025$. The spectra of Γ_c for the four cases, $\tau = \{0.01, 0.03, 0.05, 0.1\}$, are compared in Fig. 10a; in part b the ratio to the spectrum for $\tau = 0.01$ is plotted for each τ. In Fig. 11 the contours of n are shown at $t = 1025$, the actual contours for $\tau = 0.01$, and the difference from that for $\tau = 0.1$. Both figures show nonconvergence of about a few percentages over a correlation

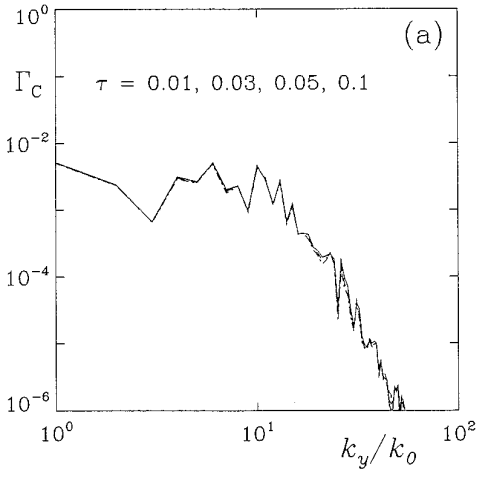

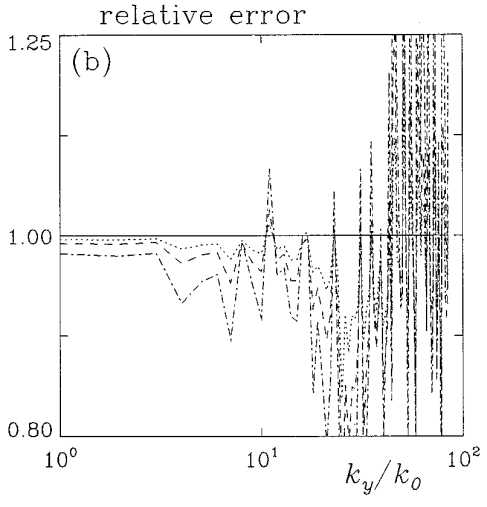

FIG. 10. (a) Spectra of the resistive dissipation rate, Γ_C, for the cases $\tau = \{0.01, 0.03, 0.05, 0.1\}$ in Fig. 8. On this scale the nonconvergence is hardly visible. (b) Ratio of $\Gamma_C(k_y)$ of each case to that for $\tau = 0.01$. The vertical scale is logarithmic. The cases are convergent to within a few percentages in the energy producing range, $k_y/k_0 < 20$ (see Fig. 5).

time. It is interesting to note the slight difference between them; the convergence in the contours is to 5% while that in the spectrum is to 10% in the energy containing range ($k_y/k_0 < 20$) and somewhat worse in the dissipation range. All of this shows the extent to which the details are important to the overall physics and the need for more than one diagnostic in assessing the performance of computational schemes.

V. CONCLUSION

Although the former implicit scheme accurately represented the physics of parallel electron dissipation in a stiffly stable way [1], the new DIRK2 scheme represents a significant improvement by making the subscheme for treating this dissipation second-order accurate. Moreover, the $E \times B$ advective terms are integrated into that subscheme, so that the difficulties with numerical error which plague high-resolution computation of the $E \times B$ shear/drift wave turbulence interaction are definitively overcome. The new scheme allows faster computation that the old, by a factor of about 7, with a convergence error of about 5% over a coherence time in most respects. Since the error in the energetics is somewhat higher, it may be more prudent in a study involving many runs to verify one or two of them at random with a lower time step in order to ensure confidence. Nevertheless, a large step toward tractability of high-resolution, three-dimensional simulation of drift wave turbulence in an inhomogeneous magnetic field has been taken.

REFERENCES

1. B. Scott, *J. Comput. Phys.* **78,** 114 (1988).
2. K. Miller, *SIAM J. Numer. Anal.* **18,** 1033 (1981).
3. For a review to 1990, see A. J. Wooton, B. A. Carreras, H. Matsumoto, K. McGuire, W. A. Peebles, Ch. P. Rirz, P. W. Terry, and S. J. Zweben, *Phys. Fluids B* **2,** 2879 (1990). The other references cited in this paragraph have appeared since.
4. Ch. P. Ritz, E. J. Powers, and R. D. Bengston, *Phys. Fluids B* **1,** 153 (1989).
5. K. W. Gentle, B. Richards, M. E. Austin, R. V. Bravanec, D. L. Brower, R. F. Gandy, W. L. Li, P. E. Phillips, D. W. Ross, W. L. Rowan, P. M. Schoch, P. M. Valanju, and A. J. Wooton, *Phys. Rev. Lett.* **68,** 2444 (1992).
6. S. V. Neudatchin, D. G. Muir, and J. D. Cordey. The time behaviour of the L-H and H-L transitions in JET, JET Preprint JET-P (93)58; *Nucl. Fusion*, to appear.
7. B. Scott, *Phys. Fluids B* **4,** 2468 (1992).
8. B. Scott, *Phys. Rev. Lett.* **65,** 3289 (1990).
9. B. Scott, *Plasma Phys. Contr. Fusion* **34,** 1977 (1992).
10. H. Sugama, M. Wakatani, and A. Hasegawa, *Phys. Fluids* **31,** 1601 (1988).
11. P. N. Guzdar, J. F. Drake, D. McCarthy, A. B. Hassam, and C. S. Liu, *Phys. Fluids B* **5,** 3712 (1993).
12. S. I. Braginskii, *Rev. Plasma Phys.* **1,** 205 (1965).
13. G. W. Hammett, M. A. Beer, W. Dorland, S. C. Cowley, and S. A. Smith, *Plasma Phys. Contr. Fusion* **35,** 973 (1993).
14. S. E. Parker and W. W. Lee, *Phys. Fluids B* **5,** 77 (1993).
15. J. F. Drake and T. M. Antonsen Jr., *Phys. Fluids* **27,** 898 (1984).
16. J. F. Drake and A. B. Hassam, *Phys. Fluds* **24,** 1262 (1981).
17. A. B. Hassam and J. F. Drake, *Phys. Fluids* **26,** 133 (1983).
18. B. Scott, *Nucl. Fusion* **32,** 873 (1992).
19. S.-T. Tsai, F. W. Perkins, and T. H. Stix, *Phys. Fluids* **13,** 2108 (1970).
20. A. Hasegawa and K. Mima, *Phys. Fluids* **21,** 87 (1978).
21. J. R. Cary and I. Doxas, *J. Comput. Phys.* **107,** 98 (1993).